Rapid Communications

Magnetically induced electric polarization in $Ba_3Fe_2O_5Cl_2$ with tunable direction in three dimensions

N. Abe,[1] S. Shiozawa,[1] K. Matsuura,[1] H. Sagayama,[2] A. Nakao,[3] T. Ohhara,[4] Y. Tokunaga,[1] and T. Arima[1]

[1]*Department of Advanced Materials Science, The University of Tokyo, Kashiwa 277-8561, Japan*

[2]*Institute of Materials Structure Science, High Energy Accelerator Research Organization, Tsukuba, Ibaraki 305-0801, Japan*

[3]*Comprehensive Research Organization for Science and Society, Tokai, Ibaraki 319-1106, Japan*

[4]*J-PARC Center, Japan Atomic Energy Agency, Tokai, Ibaraki 319-1195, Japan*

(Received 6 August 2019; revised manuscript received 25 March 2020; accepted 4 May 2020; published 21 May 2020)

The correlation between magnetism and electric polarization in a chiral insulating magnet $Ba_3Fe_2O_5Cl_2$ has been investigated. The temperature dependence of magnetic susceptibility shows an anomaly at 564 K, suggesting the onset of antiferromagnetic order of Fe^{3+} moments. Electric polarization appears in a magnetic field below T_N due to the spin-direction-dependent metal-ligand hybridization. The direction of the electric polarization can be controlled in three-dimensional space by changing the direction of an external magnetic field. This compound also shows an antiferromagnetic-to-weak-ferromagnetic transition accompanied by a structural phase transition at 140 K.

DOI: 10.1103/PhysRevB.101.180407

The coupling between crystallographic chirality and magnetism in matter has attracted much attention. Recent extensive studies show that a chiral magnet can host novel phenomena related to the relativistic spin-orbit interaction [1,2], such as the formation of a magnetic skyrmion lattice [3] and chiral soliton lattice [4], magnetochiral dichroism [5], and nonreciprocal propagations of spin waves [6]. In particular, several kinds of isotropic chiral magnetic metals have been found to be a good basis for magnetic skyrmions [7,8]. Several interesting responses such as a topological Hall effect and current-induced transport of skyrmions have been observed. Some chiral magnetic metals show relatively high magnetic transition temperatures [8], which would be useful for future technological applications. Insulating chiral magnets also exhibit interesting phenomena such as magnetoelectric [9–12] and magnetochiral effects [13]. Their magnetic transition temperatures are, however, low in most cases, because the magnetic interactions in insulating magnets are generally weaker than those in metallic magnets. Well-known exceptions are iron oxide compounds, where the magnetic transition temperature often exceeds room temperature.

We here perform magnetic and dielectric measurements, as well as x-ray and neutron diffraction measurements, of an insulating iron oxychloride $Ba_3Fe_2O_5Cl_2$. The oxychloride was first reported by Leib and Müller-Buschbaum [14], who were interested only in the structural chemistry. The crystal structure is shown in Fig. 1(a). This compound belongs to a chiral cubic space group $I2_13$ at room temperature [14]. Magnetic Fe^{3+} ions are coordinated by oxygen tetrahedra. Neighboring FeO_4 tetrahedra are linked by sharing their corners and ten FeO_4 tetrahedra form a ring structure. Since a relevant iron oxychloride $Sr_3Fe_2O_5Cl_2$ undergoes a magnetic transition at about 600 K [15], we expect that $Ba_3Fe_2O_5Cl_2$ may also have a high magnetic transition temperature.

Single crystals for magnetization measurements were grown by using a self-flux method as an early study [14]. $BaCO_3$, Fe_2O_3, and $BaCl_2 \cdot 2H_2O$ with a ratio 2:1:10 were mixed in an agate mortar and heated up to 1000 °C in a platinum crucible, then cooled down to 800 °C at a rate of 0.8 °C/h in air. Typical dimensions of the single crystals grown from the flux were $1mm^3$. Larger single crystals were grown by using the traveling solvent floating zone method with a flux of $BaCl_2$ in Ar atmosphere. $BaCO_3$, Fe_2O_3, and $BaCl_2 \cdot 2H_2O$ with a ratio of 2:1:1.5 were mixed in an agate mortar and calcined at 750 °C for 12 h in air. The powder was pressed into a thin cylinder to form feed and seed rods. The feeding speed for the rods in the floating zone melting was about 12 mm/h to reduce the evaporation of the flux. The obtained crystals were 4 cm in length and 3 mm in diameter, as shown in Fig. 1(b). A powder x-ray diffraction pattern measured by using an x-ray diffractometer (Rigaku Smart Lab) was essentially the same as an early report [14] without any impurities. The crystal principal axes were determined by Laue photography. Magnetic susceptibility was measured by using a superconducting quantum interference device magnetometer (Quantum Design MPMS-XL). Electric polarization was obtained by integrating the pyroelectric current measured by using an electrometer (Keithley 6517B). A synchrotron x-ray diffraction measurement was performed on BL-8A at the Photon Factory, Japan. Crystal structure parameters were refined by the SHLEXL2013 program [16]. An elastic neutron scattering measurement was performed on BL18 SENJU [17] at the Materials and Life Science Experimental Facility, J-PARC, Japan. Magnetic structure parameters were refined by using JANA2006 software [18].

Figures 1(b) and 1(c) show the temperature dependence of the dielectric constant and dielectric loss at several frequencies, respectively. This compound is a good insulator

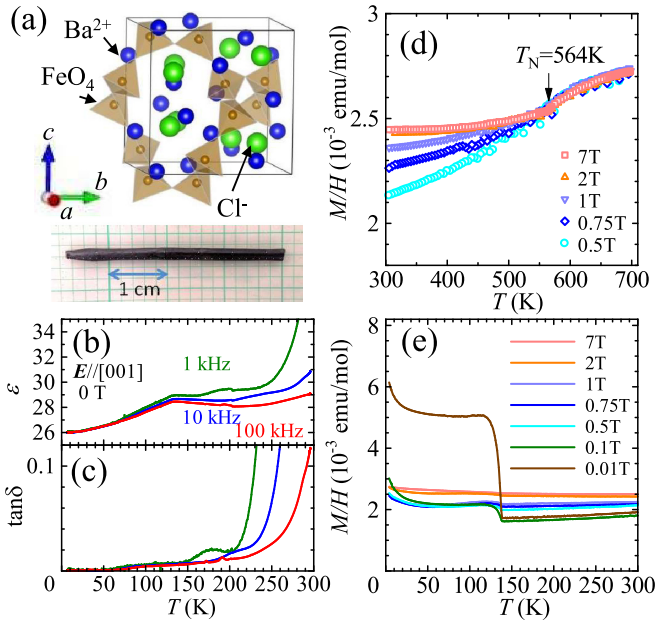

FIG. 1. (a) Crystal structure and single-crystal boule of $Ba_3Fe_2O_5Cl_2$ grown by the floating zone method. (b), (c) Temperature dependence of (b) dielectric constant and (c) dielectric loss tan δ at several electric field frequencies. In the dielectric measurement, the electric field is applied along the [001] direction. (d), (e) Temperature dependence of magnetization of an aggregate of small single crystals at several magnetic fields.

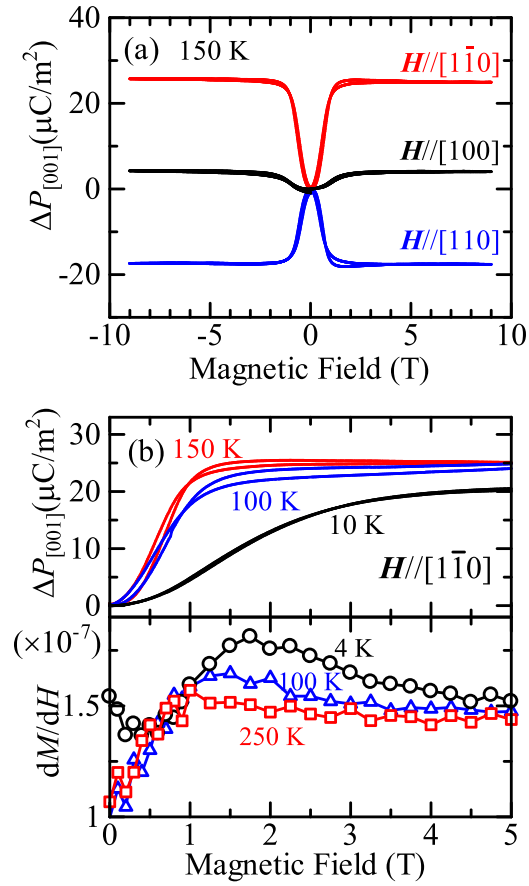

FIG. 2. (a) Magnetic field dependence of electric polarization $\Delta P_{[001]}$ along the [001] axis. The magnetic field is applied along [1$\bar{1}$0] (red), [100] (black), or [110] (blue). (b) Electric polarization $\Delta P_{[001]}$ along the [001] axis and dM/dH at several temperatures as functions of magnetic field. The magnetic field is applied in the [1$\bar{1}$0] direction.

below 200 K, however, dielectric loss rapidly increases with rising temperature above 200 K. To avoid the effects of imperfect insulation, we measure the magnetoelectric effect below 150 K. Figures 1(d) and 1(e) show the temperature dependence of magnetization (M) of an aggregate of small single crystals. The M/H-T curves show two anomalies at 564 and 140 K. It seems that $Ba_3Fe_2O_5Cl_2$ should undergo an antiferromagnetic transition at $T_N = 564$ K. The observed superlinear M/H behavior below 564 K implies some flop of antiferromagnetically aligned spin moments of Fe^{3+}. The high antiferromagnetic transition temperature may originate from the three-dimensional network of high-spin Fe^{3+} ($3d^5$) ions. The origin of the other anomaly at 140 K is discussed later.

Next, we measure the magnetic field dependence of the change in electric polarization in the [001] direction. When a magnetic field is applied in the [1$\bar{1}$0] direction at 150 K, electric polarization appears in the $+c$ direction. The electric polarization is reversed by rotating the magnetic field to the [110] direction. When the magnetic field is applied along the [100] axis, the electric polarization almost disappears. At 150 K, the value of electric polarization is saturated at about 1 T. In order to understand the relationship between the magnetic structure and induced electric polarization, we compare dM/dH and the electric polarization in a magnetic field along the [110] axis, as shown in Fig. 2(b). The electric polarization drastically increases with an increase of dM/dH up to around 1 T. In the antiferromagnetic state, the magnetic susceptibility becomes larger when the magnetic moments are oriented perpendicular to the magnetic field. Therefore, the change in dM/dH with sweeping the magnetic field is attributable to the spin-flop transition.

We also perform single-crystal neutron diffraction measurements and analyze the magnetic structure. Figure 3(a) shows the neutron diffraction pattern at 200 K for the $(h + k\ \bar{h} + k\ \bar{h})$ plane in reciprocal space. While reflections of $h + k + l =$ odd are forbidden in the body-centered lattice, $(1\bar{1}\bar{1})$ and $(3\bar{3}\bar{3})$ reflections are discernible in a low Q region at 200 K. These peaks can be ascribed to the antiferromagnetic ordering of Fe^{3+} spin moments. The magnetic reflections clearly indicate that the body-centered translation should accompany spin reversal. This situation can be realized when nearest-neighbor Fe^{3+} spins are arranged antiferromagnetically. We assume the magnetic space group $R3$ where Fe^{3+} spin moments form a simple collinear antiferromagnetic structure with spin moments along the $\langle 111 \rangle$ axis in the cubic setting. We use 523 magnetic reflections to refine the magnetic structure with $R = 13.37\%$ and $Rw = 15.96\%$. The Fe^{3+} magnetic moment is $4.028(3)\mu_B$ at 200 K, which suggests the high spin state of Fe^{3+} ($S = 5/2$).

Figure 3(c) shows possible magnetic structures when the spin moments are flopped by a magnetic field applied along the [100], [110], and [1$\bar{1}$0] directions in the cubic setting,

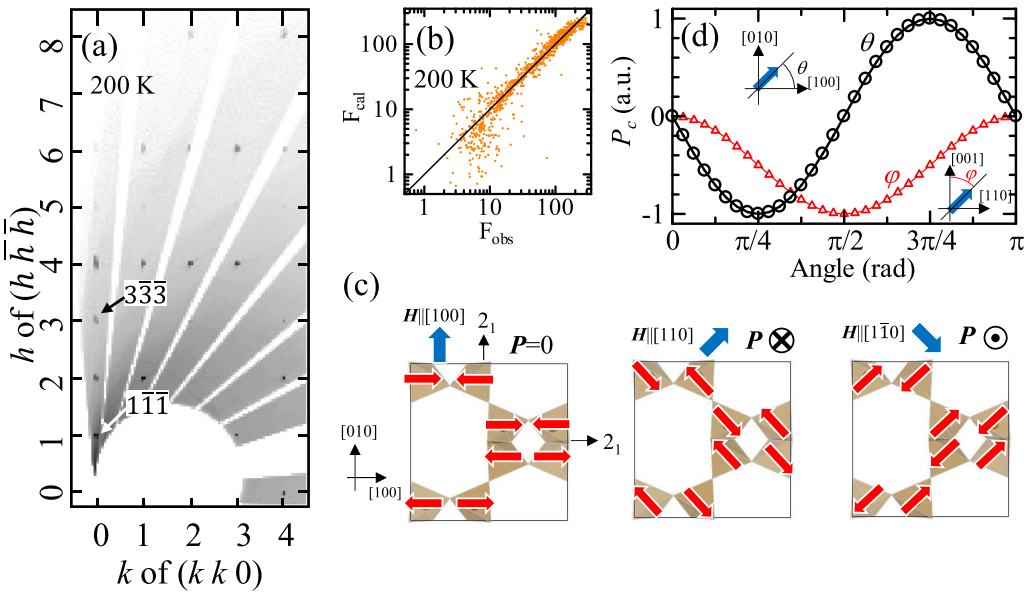

FIG. 3. (a) Single-crystal neutron diffraction pattern of $Ba_3Fe_2O_5Cl_2$ at 200 K in the $(h+k\ \bar{h}+k\ \bar{h})$ plane in reciprocal lattice space. (b) Comparison between observed and calculated intensities of magnetic reflections at 200 K. (c) Schematic illustration of the relation between the magnetic structure and induced electric polarization in magnetic fields applied along [100], [110], and [1$\bar{1}$0] directions. Red and blue arrows show Fe^{3+} spin moments and the magnetic field direction, respectively. (d) Electric polarization P_c along the [001] axis predicted by the spin-direction-dependent *p-d* hybridization model. Black circles and red triangles show the cases where the magnetic field rotate from [100] to [010] and from [001] to [110], respectively.

respectively. When a magnetic field is applied along the [100] axis, the spin moments may be oriented along the [010] or [001]. In such a case, the crystallographic 2_1 screw axes along [100], [010], and [001] may remain, and the electric polarization would not appear. On the other hand, a magnetic field applied along the [110] or [1$\bar{1}$0] axis breaks the 2_1 screw axes along the [100] and [010]. As a result, electric polarization can appear along the [001] axis. Because the cases for $\boldsymbol{H} \parallel [110]$ and $\boldsymbol{H} \parallel [1\bar{1}0]$ are related to each other by the 2_1 screw operation along the [100] axis, the direction of induced electric polarization is opposite to each other for $\boldsymbol{H} \parallel [110]$ and $\boldsymbol{H} \parallel [1\bar{1}0]$. These symmetry considerations well explain the experimental results, as shown in Fig. 2(a). The expected electric polarization is represented as $\boldsymbol{P} = a(H_yH_z, H_zH_x, H_xH_y)$.

The electric polarization generation in $Ba_3Fe_2O_5Cl_2$ can be explained by the spin-direction-dependent *p-d* hybridization model [19]. In the model, the magnetically induced component $\Delta p_{[001]}$ of the local electric dipole moment in the [001] direction at each FeO_4 tetrahedron can be expressed as

$$\Delta p_{[001]} \sim \sum_{i=1}^{4} c\boldsymbol{e}_i \cdot \boldsymbol{e}_{[001]}(\boldsymbol{e}_i \cdot \boldsymbol{s})^2. \qquad (1)$$

Here, $\boldsymbol{e}_i$ is the unit vector pointing from Fe^{3+} to the ith ligand, $\boldsymbol{e}_{[001]}$ is the unit vector in the [001] direction, $\boldsymbol{s}$ is the spin moment of Fe^{3+}, and c is a constant. Note that we assume the absence of enantiomorphic twins. Figure 3(d) shows the electric polarization as a function of magnetic field direction calculated by the model [20]. The sum of the induced polarizations of eight FeO_4 tetrahedra in a unit cell depends on the direction of the Fe^{3+} spin moment. If the spin moment rotates in the (001) plane, as shown by the black circles in Fig. 3(d), the electric polarization in the [001] direction should exhibit a sinusoidal change. The sign of $\Delta p_{[001]}$ is reversed by rotating the Fe^{3+} spin moments from parallel to [1$\bar{1}$0] to parallel to [110]. Here, the sign of $\Delta p_{[001]}$ depends only on the spin component perpendicular to [001]. In contrast, the sign of $\Delta p_{[001]}$ should be unchanged with a rotation of the spin moments in the (1$\bar{1}$0) plane, as shown by the red triangles in Fig. 3(d). These predictions are consistent with

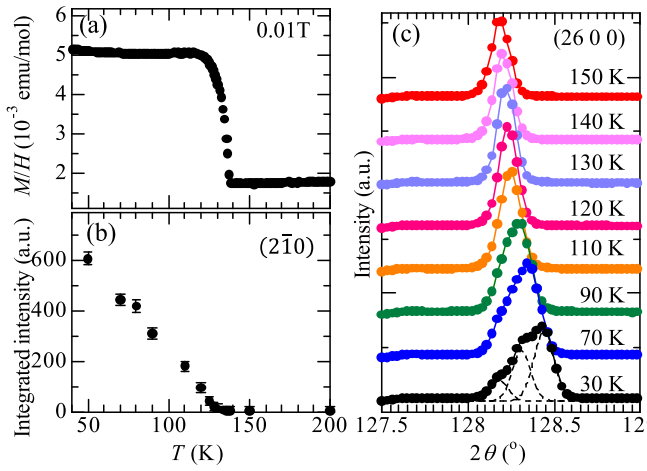

FIG. 4. (a) and (b) Temperature dependence of M/H at 0.01 T and the intensity of (2$\bar{1}$0) x-ray superlattice reflection at 0 T, respectively. (c) Profiles of (26 0 0) Bragg reflection at several temperatures. Below $T_C = 140$ K, the Bragg peak splits into three peaks along the 2θ axis with decreasing temperature. Dotted lines show Gaussian fitting of the profile at 30 K.

TABLE I. Structure parameters of $Ba_3Fe_2O_5Cl_2$ at 200 K obtained by using total 3086 reflections including 303 unique reflections. The space group is $I2_13$ (No. 199). The lattice parameter is $a = 9.9567(2)$ Å. Obtained R factors are $R = 1.14\%$ and $Rw = 2.80\%$. Goodness-of-fit indicator S (all reflections) is 1.139. Flack parameter is 0.05.

	Site	x	y	z	B_{eq}(Å^2)
Ba	12*b*	0.40554(4)	0	0.25	0.741(16)
Fe	8*a*	0.59466(6)	0.59466(6)	0.59466(6)	0.41(2)
Cl	8*a*	0.30705(1)	0.30705(1)	0.30705(1)	1.23(4)
O1	12*b*	0.1368(5)	0	0.25	1.03(8)
O2	8*a*	0.4883(3)	0.4883(3)	0.4883(3)	0.71(9)

	U_{11}(Å^2)	U_{22}(Å^2)	U_{33}(Å^2)	U_{12}(Å^2)	U_{13}(Å^2)	U_{23}(Å^2)
Ba	0.0076(3)	0.0128(3)	0.0077(3)	0.00000	0.00000	−0.00102(16)
Fe	0.0052(3)	0.0052(3)	0.0052(3)	0.0002(3)	0.0002(3)	0.0002(3)
Cl	0.0156(5)	0.0156(5)	0.0156(5)	0.0035(5)	0.0035(5)	−0.0035(5)
O1	0.013(2)	0.018(2)	0.009(2)	0.00000	0.00000	0.009(2)
O2	0.0090(11)	0.0090(11)	0.0090(11)	−0.0016(14)	−0.0016(14)	−0.0016(14)

the experimental results. The obtained electric polarization $\Delta P_{[001]} \sim 30\ \mu C/m^2$ as shown in Fig. 2(a) is comparable to that of other multiferroics with a spin-direction-dependent *p-d* hybridization mechanism [21,22]. Although the electrical resistance is too low to measure the electric polarization at room temperature at the present stage, $Ba_3Fe_2O_5Cl_2$ is a promising multiferroic operating at room temperature which is far below $T_N = 564$ K.

As shown in Fig. 1(e), $Ba_3Fe_2O_5Cl_2$ shows another magnetic transition at $T_C = 140$ K below which the spontaneous magnetization of about $3.5 \times 10^{-5}\mu_B/Fe^{3+}$ appears. In addition, the dielectric constant shows a frequency-independent anomaly near T_C, as shown in Fig. 1(b). To uncover the mechanism of the antiferromagnetic-to-weak-ferromagnetic transition, the change in crystal structure across T_C is investigated. Figures 4(a) and 4(b) show the temperature dependence of M/H at 0.01 T and the integrated intensity of $(2\bar{1}0)$ x-ray reflection, respectively. Unlike the result of the present neutron diffraction measurement, reflections with $h + k + l =$ odd are absent above T_C. The reflection condition clearly indicates that the body-centered symmetry is retained. On the other hand, reflections with $h + k + l =$ odd appear below T_C and monotonically increase in intensity with decreasing the temperature, as shown in Fig. 4(b). Moreover, (26 0 0) reflection gradually splits into three peaks in the 2θ direction with decreasing temperature below T_C, as shown in Fig. 4(c), while (h h h) reflections do not (not shown), which indicates the lowering of symmetry from cubic to orthorhombic. We conclude that the low-temperature phase belongs to the orthorhombic space group $P2_12_12_1$. Detailed crystal structure parameters at 200 and 30 K are listed in Tables I and II, respectively. We consider that the structural phase transition should arise from the structural instability common to the isostructural materials [23]. Large temperature factors B_{eq} for Cl and O1 sites at 200 K also suggest a structural instability. The decrease in thermal fluctuation induces some displacement of ions, and the structure changes from cubic to orthorhombic. As a consequence, the Fe site splits into two inequivalent sites in the low-temperature phase. Since the magnetic sublattice of the antiferromagnetic order coincides with the crystallographic Fe sublattice, some spontaneous magnetization can appear in the orthorhombic phase due to imperfect cancellation of the up- and down-spin moments. Another possible scenario is the spin canting due to the imperfect cancellation of the Dzyaloshinskii-Moriya interaction. As discussed earlier, magnetically induced electric polarization provides clear information about the spin reorientation. As shown in Fig. 2(b), the magnetoelectric effect at 100 K is similar to that at 150 K. This result implies that the direction of the spontaneous magnetization below 140 K is almost perpendicular to the spin moment. We conclude that the main origin of the spontaneous magnetization is the canting of antiferromagnetically ordered moments.

In conclusion, we have investigated the structural, magnetic, and dielectric properties of a chiral insulating magnet $Ba_3Fe_2O_5Cl_2$. The antiferromagnetic transition temperature is 564 K. The antiferromagnetic ordering in the chiral structure

TABLE II. Structure parameters of $Ba_3Fe_2O_5Cl_2$ at 30 K obtained by using total 6056 reflections including 1779 unique reflections. The space group is $P2_12_12_1$ (No. 19). Lattice parameters are $a = 9.9556(2)$ Å, $b = 9.9506(2)$ Å, and $c = 9.9468(2)$ Å. In this analysis, three domains formed by the structural phase transition from cubic to orthorhombic are considered. Isotropic thermal parameters are assumed. Obtained R factors are $R = 1.81\%$ and $Rw = 4.48\%$. Goodness-of-fit indicator S (all reflections) is 1.043. Flack parameter is 0.01.

	Site	x	y	z	B_{eq}(Å^2)
Ba1	4*a*	0.09361(14)	0.5070(4)	0.2576(2)	0.18(2)
Ba2	4*a*	0.2426(3)	0.90574(14)	0.4981(5)	0.13(2)
Ba3	4*a*	0.50966(19)	0.7508(5)	0.09425(11)	0.20(3)
Fe1	4*a*	0.4031(3)	0.5918(4)	0.4052(3)	0.12(4)
Fe2	4*a*	0.5920(3)	0.9034(3)	0.4033(4)	0.11(4)
Cl1	4*a*	0.2021(4)	0.8099(6)	0.1868(5)	0.35(9)
Cl2	4*a*	0.8156(4)	0.6966(6)	0.1996(5)	0.36(9)
O1	4*a*	0.5087(11)	0.7424(13)	0.3615(14)	0.4(2)
O2	4*a*	0.3613(12)	0.4887(11)	0.2532(12)	0.1(2)
O3	4*a*	0.2397(12)	0.6360(19)	0.4915(11)	0.7(3)
O4	4*a*	0.5050(12)	0.4858(13)	0.5162(13)	0.2(3)
O5	4*a*	0.4817(13)	0.0112(13)	0.5046(13)	0.5(3)

induces the electric polarization if the magnetic field is canted away from the cubic principal axes. A cubic-orthorhombic structure phase transition at 142 K induces a weak ferromagnetic moment.

The authors thank H. Sumi, N. Netsu, N. D. Khanh, T. Omi, and T. Yamauchi for their assistance in the experiment. This work was partly supported by Grants-in-Aid for Scientific Research (No. 26800167, No. 16H01065, and No. 18H04309). The measurements of magnetization, electric polarization, and x-ray Laue photography were performed using facilities of the Institute for Solid State Physics, The University of Tokyo. The synchrotron x-ray measurements were performed at the Photon Factory BL-8A under User Programs No. 2012S2-005. The neutron experiments were performed at the Materials and Life Science Experimental Facility of the J-PARC under User Programs No. 2014B0106. The crystal structure was drawn by using VESTA [24].

[1] I. Dzyaloshinskii, J. Phys. Chem. Solids **4**, 241 (1958).
[2] T. Moriya, Phys. Rev. **120**, 91 (1960).
[3] S. Muhlbauer, B. Binz, F. Jonietz, C. Pfleiderer, A. Rosch, A. Neubauer, R. Georgii, and P. Boni, Science **323**, 915 (2009).
[4] Y. Togawa, T. Koyama, K. Takayanagi, S. Mori, Y. Kousaka, J. Akimitsu, S. Nishihara, K. Inoue, A. S. Ovchinnikov, and J. Kishine, Phys. Rev. Lett. **108**, 107202 (2012).
[5] G. L. J. A. Rikken and E. Raupach, Nature (London) **390**, 493 (1997).
[6] S. Seki, Y. Okamura, K. Kondou, K. Shibata, M. Kubota, R. Takagi, F. Kagawa, M. Kawasaki, G. Tatara, Y. Otani, and Y. Tokura, Phys. Rev. B **93**, 235131 (2016).
[7] T. Tanigaki, K. Shibata, N. Kanazawa, X. Yu, Y. Onose, H. S. Park, D. Shindo, and Y. Tokura, Nano Lett. **15**, 5438 (2015).
[8] Y. Tokunaga, X. Z. Yu, J. S. White, H. M. Rønnow, D. Morikawa, Y. Taguchi, and Y. Tokura, Nat. Commun. **6**, 7638 (2015).
[9] S. Seki, S. Ishiwata, and Y. Tokura, Phys. Rev. B **86**, 060403(R) (2012).
[10] E. Ruff, S. Widmann, P. Lunkenheimer, V. Tsurkan, S. Bordács, I. Kézsmárki, and A. Loidl, Sci. Adv. **1**, e1500916 (2015).
[11] Y. Fujima, N. Abe, Y. Tokunaga, and T. Arima, Phys. Rev. B **95**, 180410(R) (2017).
[12] K. Kimura, P. Babkevich, M. Sera, M. Toyoda, K. Yamauchi, G. S. Tucker, J. Martius, T. Fennell, P. Manuel, D. D. Khalyavin, R. D. Johnson, T. Nakano, Y. Nozue, H. M. Rønnow, and T. Kimura, Nat. Commun. **7**, 13039 (2016).
[13] N. Nakagawa, N. Abe, S. Toyoda, S. Kimura, J. Zaccaro, I. Gautier-Luneau, D. Luneau, Y. Kousaka, A. Sera, M. Sera, K. Inoue, J. Akimitsu, Y. Tokunaga, and T. Arima, Phys. Rev. B **96**, 121102(R) (2017).
[14] W. Leib and Hk. Müller-Buschbaum, Z. Anorg. Allg. Chem. **521**, 51 (1985).
[15] C. S. Knee, M. A. L. Field, and M. T. Weller, Solid State Sci. **6**, 443 (2004).
[16] G. M. Sheldrick, Acta Crystallogr., Sect. A **64**, 112 (2008).
[17] T. Ohhara, R. Kiyanagi, K. Oikawa, K. Kaneko, T. Kawasaki *et al.*, J. Appl. Crystallogr. **49**, 120 (2016).
[18] V. Petříček, M. Dušek, and L. Palatinus, Z. Kristallogr. Cryst. Mater. **229**, 345 (2014).
[19] T. Arima, J. Phys. Soc. Jpn. **76**, 073702 (2007).
[20] See Supplemental Material at http://link.aps.org/supplemental/10.1103/PhysRevB.101.180407 for the calculation of electric polarization in $Ba_3Fe_2O_5Cl_2$.
[21] T. Kimura, J. C. Lashley, and A. P. Ramirez, Phys. Rev. B **73**, 220401(R) (2006).
[22] H. Murakawa, Y. Onose, S. Miyahara, N. Furukawa, and Y. Tokura, Phys. Rev. Lett. **105**, 137202 (2010).
[23] W. Leib and Hk. Müller-Buschbaum, Rev. Chim. Miner. **23**, 760 (1986).
[24] K. Momma and F. Izumi, J. Appl. Crystallogr. **44**, 1272 (2011).